Role of Heterogeneous Reactions in the Atmospheric Oxidizing Capacity in Island Environments

Chaoyang Xue, Hui Chen, Max Mcgillen, Hang Su, Yafang Cheng, Jörg Kleffmann, Guo Li, Mathieu Cazaunau, Aurélie Colomb, Jean Sciare, et al.

Environmental Science & Technology

pubs.acs.org/est

Article

Role of Heterogeneous Reactions in the Atmospheric Oxidizing Capacity in Island Environments

Chaoyang Xue,* Hui Chen, Max R. McGillen, Hang Su, Yafang Cheng, Jörg Kleffmann, Guo Li, Mathieu Cazaunau, Aurélie Colomb, Jean Sciare, Langley DeWitt, Nicolas Marchand, Roland Sarda-Esteve, Jean-Eudes Petit, and Alexandre Kukui*

Cite This: https://doi.org/10.1021/acs.est.4c11647

Read Online

ACCESS | Metrics & More | Article Recommendations | Supporting Information

ABSTRACT: The source of nitrous acid (HONO) and its importance in island or marine environments are poorly understood. Herein, based on comprehensive field measurements at a hilltop on Corsica Island, we find an inverse diel variation of HONO with higher concentrations during daytime. Night-time HONO budget analysis indicates significant HONO formation during air mass transport along the hillside. In the daytime, although photosensitized NO_2 uptake on the ground and NO + OH make considerable contributions (26% and 5%, respectively), a large part of HONO formation (67%, 320 pptv h^{-1}) still cannot be explained with state-of-the-art parametrization. Nevertheless, photosensitized heterogeneous NO_2 reactions are likely to account for the missing source, due to underestimation of the source by typical parametrizations at low NO_2 levels. Furthermore, we demonstrate a significant role of HONO formation as a OH primary source at this island site, with a OH production rate exceeding one-fourth of that of O_3 photolysis. Our findings underscore a potential role of heterogeneous surface reactions in the oxidizing capacity of the island environments.

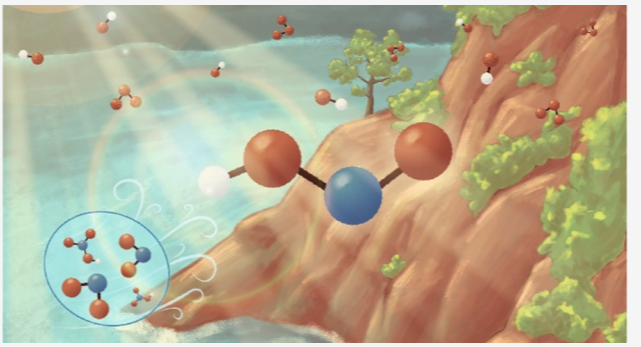

KEYWORDS: *nitrous acid, heterogeneous reactions, NO_2 conversion, nitrate photolysis, island environments*

1. INTRODUCTION

While the atmospheric chemistry related to nitrous acid (HONO) has been studied for more than four decades,[1] many uncertainties remain regarding its formation. It is important to understand how HONO is formed because of its significant impact on the oxidizing capacity of the lower troposphere by producing hydroxyl radical (OH) and follow-up impact on air pollution and climate.[2,3] Hence, to identify major HONO sources, many field campaigns were conducted worldwide, most focusing on continental regions.[2,4,5] However, only a few measurements have been targeted at the marine atmosphere where OH levels significantly affect the lifetime of greenhouse gases such as methane,[6] indicating the necessity of studying OH sources in marine environments. Besides a few studies using aircraft/ship platforms,[7,8] measurements on islands (or coastal areas) can also provide insights into marine atmospheric chemistry.[9−14]

Compared to high-NO_x environments (e.g., urban regions) where HONO formation and its impact have been well established, HONO over islands is poorly studied and it typically shows a different diel variation, i.e., higher levels in the day but lower levels at night.[9−11] On the one hand, this indicates the non-negligible contribution of HONO to OH over the island and the surrounding ocean, while the contribution over continental regions is already well established. Furthermore, this may provide insights into chemical processes or boundary layer dynamics driving island HONO formation, which need to be further explored by field measurements. Notably, different HONO formation paths have been proposed for HONO formation at several island/coastal sites. In Cyprus, Meusel et al.[12] observed higher HONO levels under low-RH than high-RH conditions, which was attributed to possible soil emissions based on laboratory experiments. At the Cape Verde CVAO site, Crilley et al.[11] obtained a daytime minimum for ocean-derived HONO of 0.23 pptv, which was much lower than their measured HONO. Their results suggest a potential role of particulate nitrate (pNO_3) photolysis but a minor role of the ocean surface in HONO formation, which was different from a previous study in a more polluted marine atmosphere.[13] In Bermuda, Zhu et

Received: October 27, 2024
Revised: January 13, 2025
Accepted: January 14, 2025

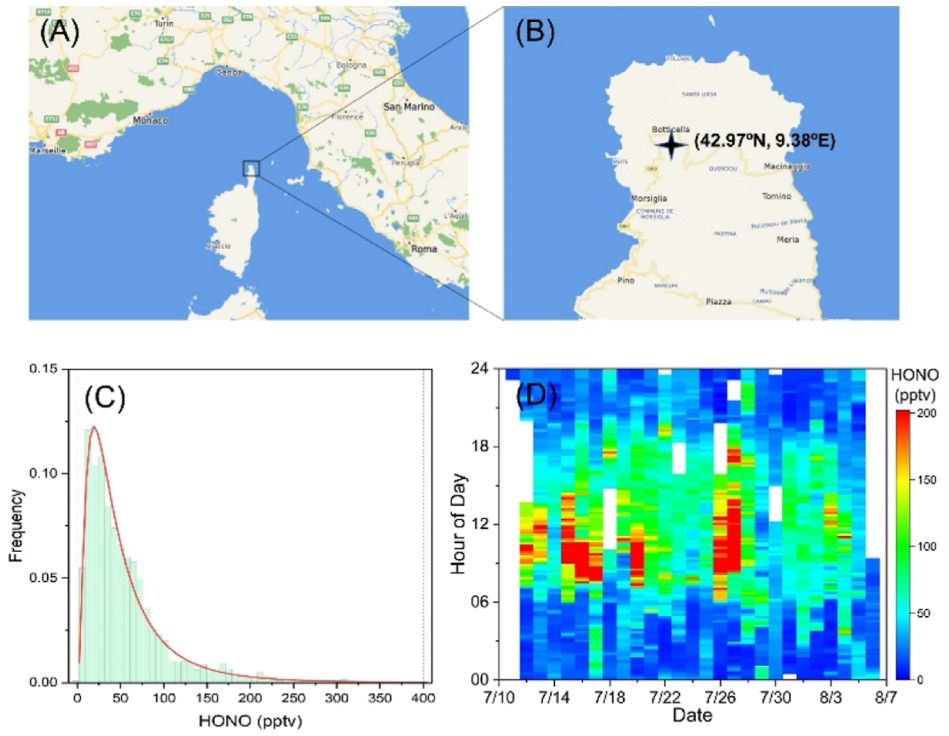

Figure 1. (A) Location of Corsica Island (Map copyright © 2022 Microsoft); (B) location of the measurement site (black cross); (C) histogram of the measured HONO data; and (D) time series of 10 min average HONO measurements during the ChArMEx campaign.

al.[14] observed higher levels of HONO and $HONO/NO_2$ in land cases than in sea cases but similar levels of pNO_3 in both cases, indicating the important impacts of the land surface rather than pNO_3 on HONO formation. Moreover, the HONO production unaccounted by NO_x or pNO_3-related processes showed a significant positive correlation with daily average HNO_3, suggesting photolysis of adsorbed HNO_3 on the land surface as the possible source.[14] Therefore, the understanding of HONO formation mechanisms over islands is still poorly understood. Comprehensive field measurements are needed to address the discrepancy in understanding HONO formation in island environments and its potential impact on the marine atmosphere.

In this study, within the framework of ChArMEx (the Chemistry and Aerosol Mediterranean Experiment), we conducted an extensive range of atmospheric measurements on Corsica. These measurements encompass HONO, various other trace gases, atmospheric radicals, and aerosol size and composition. The comprehensive data set allows a detailed analysis of the HONO budget. Combined with state-of-the-art HONO source parametrizations and box model simulations, we provide new insights into HONO chemistry in island environments: (1) HONO may contribute significantly to daytime OH production and (2) heterogeneous NO_2 reactions are expected to dominate the missing HONO source.

2. METHOD

2.1. ChArMEx Campaign. Data used in this study were obtained during the ChArMEx SOP2 (special observation period-2, https://mistrals.sedoo.fr/ChArMEx/, last access: 24 May 2023) field campaign, which was conducted in July and August 2013.[15,16] Comprehensive measurements were conducted on the top of a hill (altitude: ~530 m above sea level) in Corsica, France (42.97°N, 9.38°E, Figure 1A,B). It is about 6.0, 4.5, and 2.5 km from the sea in the east, north, and west directions, respectively.

2.2. Instrumentation. Table S1 shows the instruments providing major measurements used in this study. The instruments were placed in several containers with a distance of less than 50 m between each other. Briefly, HONO was measured by a wet chemical method (LOPAP-03, QUMA GmbH, Germany),[17] which has been validated in a smog chamber and the ambient atmosphere by intercomparison with the DOAS technique.[18] One potential interference (and/or HONO source) from the hydrolysis of nitrosyl chloride (ClNO) is discussed in Section 1 in the Supporting Information. The external sampling unit of LOPAP was installed on the top of a container (2.5 m above the ground level). Zero calibration was automatically conducted 2−3 times per day through sampling synthetic air (N_2/O_2 = 4:1). Liquid calibration was regularly carried out by a diluted nitrite solution in the sampling reagent under zero air. The measurement uncertainty was 10%, and the detection limit was a few parts per trillion (pptv) during this campaign. OH radicals were measured by a CIMS with detection limits of $5.0 \cdot 10^5$ and $2.0 \cdot 10^5$ molecules cm^{-3} for daytime and night-time measurements.[16,19] Aerosol number size distributions in the ranges of 109−496 and 542−19,500 nm were measured by an SMPS TSI 3080 associated with a CPC TSI 3010 and an aerodynamic particle sizer APS TSI 3321, respectively. Aerosol composition and gas-phase HNO_3/HCl were quantified by an Aerodyne HR-ToF-AMS and a wet denuder-ion chromatography (WAD-IC) system,[20] respectively. O_3 was measured by a commercial analyzer based on UV absorption (Thermo Fisher Scientific, Model 49i). Meteorology and J values were measured by an autometaphysical station and a spectral radiometer (Meteorologie Consult GmbH 6007), respectively. NO and NO_2 were measured by the ECO PHYSICS $CraNO_x$

https://doi.org/10.1021/acs.est.4c11647
Environ. Sci. Technol. XXXX, XXX, XXX−XXX

Table 1. Parameters Used in the HONO Source/Sink Equations[a]

parameter	meaning	value (range)	references
$J(HONO)$	HONO photolysis rate	measured, in s^{-1}	
$k_{HONO+OH}$	HONO + OH reaction rate coefficient	$6.0{\cdot}10^{-12}$ cm3 $molecule^{-1}$ s^{-1}	1
$v_{deposition}$	deposition velocity of HONO	0.5 (0.1−2) cm s^{-1}[b]	2
MLH_{HONO}	mixing layer height for HONO	50 (10−200) m[c]	3
k_{NO+OH}	NO + OH reaction rate coefficient	$9.8{\cdot}10^{-12}$ cm^3 $molecule^{-1}$ s^{-1}	1
$v(NO_2)$	mean NO_2 molecular speed	calculated by eq-7, in m s^{-1}	
R	ideal gas constant	8.314 kg m^2 s^{-2} mol K	
T	temperature	measured, in K	
M	NO_2 molar mass	0.046 kg mol^{-1}	
S/V	surface-to-volume ratio	calculated by eq-8[d], in m^{-1}	
SEF	surface enhancement factor[e]	5 or 2.7	
γ_{NO2_ground}	NO_2 uptake coefficient on ground surfaces	$1.5{\cdot}10^{-6}$ ($<10^{-6}$−10^{-5})	4
$(S/V)_{aerosol}$	aerosol surface density	measured, in m^{-1}	
$\gamma_{NO2\_aerosol}$	NO_2 uptake coefficient on aerosol surfaces	$1.5{\cdot}10^{-6}$ ($1{\cdot}10^{-7}$−$1.6{\cdot}10^{-5}$)	5
γ_{NO2+hv_ground}	photosensitized NO_2 uptake coefficient on ground surfaces	$2{\cdot}10^{-5}$ ($4{\cdot}10^{-6}$−$5{\cdot}10^{-5}$)	6
$J(NO_2)$	NO_2 photolysis rate	measured, in s^{-1}	
$\gamma_{NO2+hv\_aerosol}$	photosensitized NO_2 uptake coefficient on aerosol surfaces	$2{\cdot}10^{-5}$ (10^{-6}−10^{-3})	6
$J(HNO_3)$	HNO_3 photolysis rate	measured	
EF	enhancement factor of pNO_3 photolysis compared to $J(HNO_3)$	7 (1−700)	7
ϕ	HONO yield	0.5 or 1[f]	

[a]Value and Range represent the used value in this study and the reported range in the literature. Reference 1: the IUPAC Task Group on Atmospheric Chemical Kinetic Data Evaluation, values at 298 K, see https://iupac.aeris-data.fr (last access: 17 August 2023); 2:[31−34]; 3:[28,33,35]; 4:[33,36−38] and this study; 5:[33,36,37]; 6:[5,36,39−43]; and 7:[8,44−46]. [b]A value (0.5 cm s^{-1}) close to the lower limit is used because a lower MLH than boundary layer height (BLH) is used in the parametrization. [c]MLH rather than marine BLH should be used here because measurements are conducted near the ground surface. Using the BLH would strongly underestimate the impact of near-ground processes like heterogeneous production and deposition losses; we note that a constant MLH used here may cause uncertainties in ground-derived HONO sources. [d]Projected geometric surface area (1 m^2 m^{-2}) is used to simplify S_{ground}/V; the use of geometric surface area results in higher uptake coefficients compared to laboratory data. [e]Similar to previous studies, surface enhancement factor (SEF) is not considered in the model parametrization in the base scenario; however, Section 3.3 explains that SEF should be taken into account. [f]Here, we applied HONO yields (ratio between HONO desorbed from and formed on the surface) of 0.5 for dark NO_2 conversion and 1 for daytime photosensitized reactions.

II instrument, with a detection limit of ∼30 pptv. The NO_2 channel of the CraNO$_x$ II instrument is equipped with a photolytic blue light converter, which uses near-UV light to convert NO_2 to NO before being detected, largely reducing interference from other odd nitrogen (NO_y) species on the NO_2 measurements.

2.3. Pseudo-Steady-State Approach. During the daytime, the relaxation of HONO concentration to pseudo-steady-state (PSS) conditions is reached on a scale of the HONO lifetime (τ(HONO), e.g., 10 min at noon, Figure S1).[6,21] Therefore, for a homogeneously mixed atmosphere, such as the marine atmosphere, forest atmosphere, rural sites, etc., the PSS approach is typically used for daytime HONO analysis.[21,22] In island regions, the underlying surface switches between land and ocean, which may significantly affect the composition of the corresponding boundary layer air masses due to variations of surface emissions, heterogeneous processes, and mixing. Therefore, when the contact time of the observed air mass with the land surface (t_{land}) is shorter than that of τ(HONO), PSS conditions may not be achieved. For the daytime HONO budget analysis, data obtained during days with $t_{land}<\tau$(HONO) were filtered out to guarantee the validity of the PSS approach. In this study, t_{land} is estimated based on the wind speed (WS) and the distance to the sea in this wind direction, as demonstrated in detail by Kukui et al.[16] As shown in Figure S1D, the calculated t_{land} is generally higher than τ(HONO), with exceptions mainly on 14, 23, 24, 25, 29, and 30 July and 6 August 2013 (therefore defined as t_{land} < τ(HONO) days).

2.4. Equations for the HONO Budget. During the day, when PSS is achieved, the HONO budget can be expressed by the following equation

$$L_{HONO+hv} + L_{HONO+OH} + L_{deposition} = P_{NO+OH} + P_{NO_2\_ground} + P_{NO_2\_aerosol} + P_{NO_2+hv\_ground} + P_{NO_2+hv\_aerosol} + P_{pNO_3+hv} + P_{unknown} \quad (1)$$

In this equation, $L_{HONO+hv}$, $L_{HONO+OH}$, and $L_{deposition}$ represent the HONO loss through photolysis, reaction with OH, and deposition, respectively. P_{NO+OH}, P_{NO2_ground}, $P_{NO2\_aerosol}$, P_{NO2+hv_ground}, $P_{NO2+hv\_aerosol}$, $P_{pNO3+hv}$, and $P_{unknown}$ denote the HONO production through the gas-phase reaction of NO + OH, NO_2 uptake on the ground surface, NO_2 uptake on the aerosol surface, photosensitized NO_2 uptake on the ground surface, photosensitized NO_2 uptake on the aerosol surface, particulate nitrate photolysis, and unknown sources, respectively. As shown in Figure S2, the observed NO and NO_2 values were generally lower than 0.4 and 1.0 ppbv, respectively, with only several sharp and short spikes possibly resulting from car exhaust or occasional local anthropogenic emissions. Biomass burning (BB) emissions could be an important or dominant HONO source in relatively fresh plumes in the downwind areas of the BB locations.[23−25] At the Corsica site, potential BB events were not often and were not large during the measurement period (see Figure S3). Moreover, the majority of air mass originated from the ocean rather than from the downwind areas of the potential BB evens (Figure S5A). Therefore, direct HONO emissions from

https://doi.org/10.1021/acs.est.4c11647
Environ. Sci. Technol. XXXX, XXX, XXX−XXX

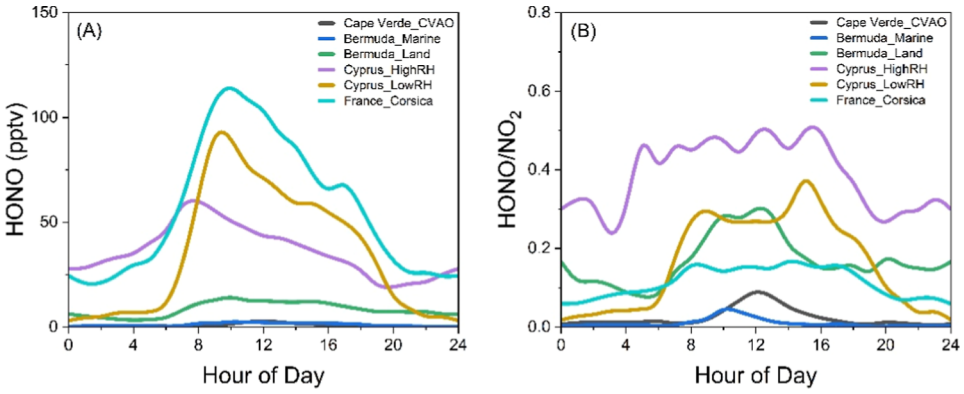

Figure 2. Diel variations of (A) HONO and (B) $HONO/NO_2$ measured at four island sites worldwide: Cyprus (under low- and high-RH conditions), the Cape Verde Atmospheric Observatory (Cape Verde_CVAO), Bermuda (land and marine cases), and Corsica (France_Corsica).

combustion processes and photolysis of gas-phase nitro compounds[26] are expected to be of minor importance at this site and have been excluded from consideration. Note that those processes may contribute to the observed HONO indirectly by contributing to NO_x on a regional scale. Unknown sources could result from soil emissions, acid displacement, photolysis of absorbed nitrate, and underestimated sources, as described in eq 1. Section 3.5 conducts detailed analyses and discussions to identify the major unknown source.

HONO sinks and sources can be parametrized according to the following equations[27,28] with the used parameters explained in Table 1. Besides calculating HONO production and loss rates, the parametrization scheme can be further used in box models to simulate HONO concentrations (see Text S1 in the Supporting Information). Note that the uptake on the aerosol surface is not included in the parametrization as a HONO sink due to its low contribution during daytime.[29,30]

$$L_{\mathrm{HONO+hv}} = [\mathrm{HONO}]\bullet J(\mathrm{HONO}) \tag{2}$$

$$L_{\mathrm{HONO+OH}} = k_{\mathrm{HONO+OH}}\bullet[\mathrm{HONO}]\bullet[\mathrm{OH}] \tag{3}$$

$$L_{\mathrm{deposition}} = \frac{v_{\mathrm{deposition}}}{\mathrm{MLH}_{\mathrm{HONO}}}\bullet[\mathrm{HONO}] \tag{4}$$

$$P_{\mathrm{NO+OH}} = k_{\mathrm{NO+OH}}\bullet[\mathrm{NO}]\bullet[\mathrm{OH}] \tag{5}$$

$$P_{\mathrm{NO_2\_ground}} = \frac{v(\mathrm{NO_2})\bullet[\mathrm{NO_2}]}{4}\bullet(S/V)_{\mathrm{ground}}\bullet\gamma_{\mathrm{NO_2\_ground}}\bullet\phi \tag{6}$$

$$\mathrm{v}(\mathrm{NO_2}) = \sqrt{\frac{8RT}{\pi M}} \tag{7}$$

$$(S/V)_{\mathrm{ground}} = \frac{1}{\mathrm{MLH}_{\mathrm{HONO}}} \tag{8}$$

$$P_{\mathrm{NO_2\_aerosol}} = \frac{\mathrm{v}(\mathrm{NO_2})\bullet[\mathrm{NO_2}]}{4}\bullet(S/V)_{\mathrm{aerosol}}\bullet\gamma_{\mathrm{NO_2\_aerosol}}\bullet\phi \tag{9}$$

$$P_{\mathrm{NO_2+hv\_ground}} = \frac{\mathrm{v}(\mathrm{NO_2})\bullet[\mathrm{NO_2}]}{4}\bullet(S/V)_{\mathrm{ground}} \bullet\gamma_{\mathrm{NO_2+hv\_ground}}\bullet\frac{J(\mathrm{NO_2})}{0.005s^{-1}}\bullet\phi \tag{10}$$

$$P_{\mathrm{NO_2+hv\_aeorosol}} = \frac{\mathrm{v}(\mathrm{NO_2})\bullet[\mathrm{NO_2}]}{4}\bullet(S/V)_{\mathrm{aerosol}} \bullet\gamma_{\mathrm{NO_2+hv\_aeorosol}}\bullet\frac{J(\mathrm{NO_2})}{0.005s^{-1}}\bullet\phi \tag{11}$$

$$P_{\mathrm{pNO_3+hv}} = [\mathrm{pNO_3}]\bullet J(\mathrm{HNO_3})\bullet\mathrm{EF}\bullet\phi \tag{12}$$

3. RESULTS AND DISCUSSION

3.1. Field Measurements. Figure S4 shows the meteorological conditions during this campaign. Ambient temperature was generally within the range of 18−30 °C, with exceptions reaching ∼30 °C during 26−28 July. Atmospheric relative humidity (RH) was around 60% in the daytime and above 90% at night. Low RH levels were observed typically along with low-speed or northern winds. Southwest was the dominant wind direction (Figure S5A), with wind speeds generally lower than 5 m s^{-1}. Strong southwestern winds of >5 m s^{-1} were observed on July 23, 24, and 30.

The measured HONO varied in the range of 2−400 pptv (Figure 1C), with an average of 56 ± 51 pptv and a median of 41 pptv. In general, much higher HONO levels were observed during the day than at night. Daily peaks were normally between 100 and 200 pptv, occurring at around 10:00−14:00 (Figure 1D). High HONO levels above 90 pptv are observed only in some east- and northeast-originated air masses, which is similar to the distributions of high NO_x (east and northeast) but opposite to high pNO_3 (southwest, Figure S5). In terms of average diel variation (Figure S6), HONO measured at this site is low and mostly stable (<30 pptv) at night and starts to increase after sunrise. It shows a peak of 127 pptv at 9:50, which is similar to that of NO_2 variations (peak at 10:10, Figure S6). Similar reverse diel variation has also been observed at other sites, which is discussed in detail in Sections 3.2 and 3.7.2.

3.2. Comparison with Other Coastal/Island Measurements. Figure 2 shows the derivative variations of HONO and $HONO/NO_2$ measured at four island sites worldwide (Table S2). The levels of HONO observed at those sites are different, varying from several to hundreds of pptv. However, their diurnal profiles behave similarly, with higher levels during the day than those at night. In particular, the France_Corsica site shows the highest daytime HONO levels among those sites and exhibits very similar levels and variations to those in Cyprus under low-RH conditions.

https://doi.org/10.1021/acs.est.4c11647
Environ. Sci. Technol. XXXX, XXX, XXX−XXX

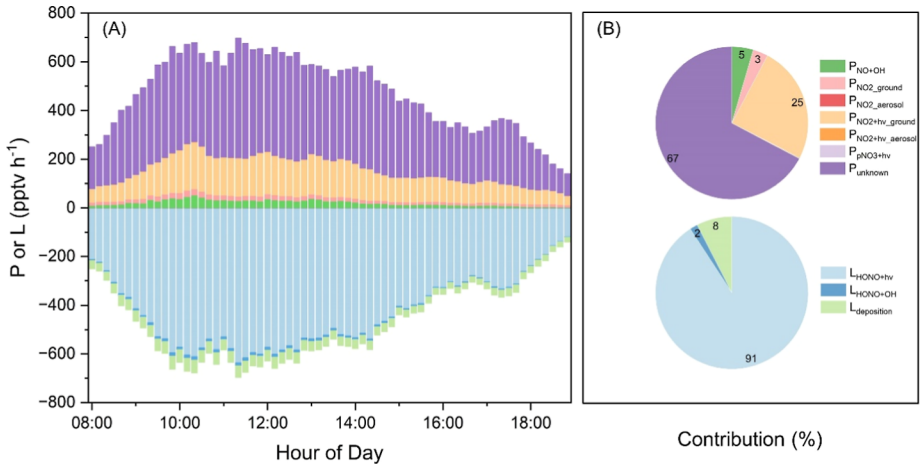

Figure 3. (A) Average diurnal profiles of daytime HONO formation (P) or loss (L) rates through different sources and sinks and (B) their relative contributions averaged over the daytime. $P_{unknown}$ was calculated according to the pseudo-steady state ($P = L$). In panel B, labels are not shown if the percentage is less than 1%.

Similar to HONO, the HONO/NO_2 ratios at all four of these sites perform a similar variation, with persistently higher levels during the day than at night. While the higher levels of daytime HONO/NO_2 (10−50%) at those sites than most inland measurements (<20%)[28,47−50] indicate the dominant role of secondary HONO formation, the significant difference in HONO/NO_2 levels at the four island/coastal sites indicates the complexity of the relationship between HONO and its potential precursor NO_2.

3.3. Night-Time HONO Budget. At night, the observed average HONO/NO_x ratio (9.3%) is much higher than that in vehicle exhaust (~1%) potentially from pass-by vehicles (not frequent). While the HONO/NO_x ratio in BB emissions could be high,[46,51,52] we have demonstrated that it is not a significant source at this site (see Section 2.4). The two findings above suggest the dominant role of secondary HONO formation.

Considering that our measurement site is on a small hill of ~530 m altitude above sea level, the night-time mountain breeze (downslope wind) may affect the observations. Assuming that the night-time mountain breeze dominates the air mass flow, the observed HONO would remain close to the level in the upper boundary layer/residual layer. However, the observed night-time HONO at the Corsica site reached about 30 pptv, which is much higher than that for the upper boundary layer/residual layer (a few pptv),[46,51,52] indicating that air mass arriving at the measurement site was not purely from those areas. Indeed, the upslope transport could be initialized by regional winds mainly from the southwest direction (distance to sea = 3.1 km) overwhelming the mountain breeze downslope air transport. And in fact, strong winds with wind speeds of 3−6 m s^{-1} were frequently observed during the nighttime (Figure S7A). Significant impact of upslope transport as well as the HONO production during the transport process on the observed HONO was also observed in our previous measurements at the summit of Mt. Tai (~1500 m above sea level).[53] As the hill at the Corsica site is much lower and smaller than that at Mt. Tai, a weaker mountain breeze can be expected at the Corsica site, making it easier to be overwhelmed by the regional winds.

The strong winds also lead to a t_{land} of 9−17 min, much smaller than the long HONO lifetime of around 2.7 h (against deposition and OH oxidization), indicating that the composition of the air arriving at the measurement site was influenced by its presence over both sea and the island. As the HONO concentration level of a few pptv typically observed for marine air mass[11,14] is about 1 order of magnitude lower than that observed at the Corsica site (~30 pptv), the HONO production during the upslope transport was likely the major contributor to the observed HONO at the Corsica site.

From 20:00 to 4:00, HONO levels are almost constant ($\frac{\Delta HONO}{\Delta t} = 0$), indicating the equality of sources and sinks, as shown in the equation below

$$L_{HONO+OH} + L_{deposition} = P_{NO+OH} + P_{NO2\_ground} + P_{NO2\_aerosol} \quad (13)$$

The average $L_{HONO+OH}$, $L_{deposition}$, P_{NO+OH}, and $P_{NO2\_aerosol}$ during 20:00−4:00 are $6.9{\cdot}10^{-3}$, 8.3, 0.02, and 0.01 pptv h^{-1}, respectively, deriving a P_{NO2_ground} of 8.3 pptv h^{-1}, indicating the dominant role of NO_2 conversion on the ground surface in night-time HONO formation. Combined with eq 6, we obtain an uptake coefficient γ_{NO2_ground} of $7.3{\cdot}10^{-6}$, which is at a relatively high level compared to previously reported ones (Table 1). This is likely due to the underestimation in $(S/V)_{ground}$ as only the projected geometric surface area was used to describe HONO formation on ground surfaces (see eq 8). If, e.g., an SEF of 5 is considered, $\gamma_{NO2+h\nu\_ground}$ of $1.5{\cdot}10^{-6}$ would also well describe the observations. This is quite reasonable considering that the true ground surface is not perfectly flat but instead exhibits vertical structures (such as stones, cracks, etc.) and significant porosity (e.g., large pores in the top layer of the soil, accessible for NO_2 uptake), which could easily lead to an SEF of up to 5. During the daytime, the SEF is expected to be smaller for photochemistry as not all surfaces are exposed to solar radiation. Therefore, the SEF should be factored into the calculation of $(S/V)_{ground}$, as shown in the following equation

$$(S/V)_{ground} = \frac{1}{MLH_{HONO}} \bullet SEF \quad (14)$$

Figure S8 shows the sensitivity of γ_{NO2_ground} to the influencing factors, $v_{deposition}$, MLH, and $\gamma_{NO2\_aerosol}$. Within the typical variation ranges of MLH or $\gamma_{NO2\_aerosol}$, γ_{NO2_ground} does not vary much around $1.5{\cdot}10^{-6}$. In contrast, γ_{NO2_ground} is directly proportional to the used $v_{deposition}$, leading to γ_{NO2_ground}

https://doi.org/10.1021/acs.est.4c11647
Environ. Sci. Technol. XXXX, XXX, XXX−XXX

variations by an order of magnitude for a typical $v_{deposition}$ range. Other uncertainties could originate from the HONO yield as a HONO yield of 50% is used to represent all NO_2-to-HONO conversion on the ground surface, including hydrolysis and, more importantly, the redox reactions.[33,38,54−56]

3.4. Daytime HONO Budget. Figure 3 illustrates the average diurnal profiles of HONO formation and loss rates during the daytime. It is clear that photolysis dominates daytime HONO loss, with a contribution of 91%, while deposition and reaction with OH contribute the rest. Among the six sources, $P_{NO2+h\nu\_ground}$ makes the largest contribution of 25%, followed by P_{NO+OH} (5%) and P_{NO2_ground} (3%). Other three sources, including $P_{NO2+hv\_aerosol}$, $P_{NO2\_aerosol}$, and $P_{pNO3+h\nu}$, contribute less than 1%. Even with the upper limits of $\gamma_{NO2+hv\_aerosol}$ and EF of $1.0{\cdot}10^{-3}$ and 700, respectively, the contribution of $P_{NO2+hv\_aerosol}$ or $P_{pNO3+h\nu}$ is still less than 8%.

With similar parametrizations as used here, HONO observations at inland sites could be generally explained.[27,28] However, at this island site, the sum of the total HONO formation from the above-mentioned six sources is still much lower than the needed strength that can account for total HONO loss, which is in agreement with model results (see Text S2 in the Supporting Information for the description of the used model) that the modeled HONO concentration is lower than observations (Figure S9). This leads to a large unknown source ($P_{unknown}$), varying from 90 to 490 pptv h^{-1}, with an average of 318 ± 101 pptv h^{-1} (Figure 3). Interestingly, $P_{unknown}$ shows asymmetric diurnal profiles compared to the diurnal profile of radiation, e.g., J(HONO) (Figure S10), with higher values in the morning compared to the afternoon, which is similar to the diurnal profiles of NO_2 (Figure S6) and $P_{NO2+h\nu\_ground}$ (Figure 3).

3.5. Potential Sources to Explain $P_{unknown}$. *3.5.1. NO_2 Uptake on the Ground Surface.* With a laboratory-determined $\gamma_{NO2+h\nu\_ground}$ of $2{\cdot}10^{-5}$ from Stemmler et al. (2006), $P_{NO2+h\nu\_ground}$ appears similar to $P_{unknown}$ in variation but ∼2 times lower in strength (Figure 3A). Moreover, as shown in Figure 4, high correlations between $P_{unknown}$ and NO_2 (r = 0.74), between $P_{unknown}$ and $NO_2{\cdot}J(NO_2)$ (r = 0.89), and between $P_{unknown}$ and $P_{NO2+h\nu\_ground}$ (r = 0.989) indicate that a larger $\gamma_{NO2+h\nu\_ground}$ could help to explain the $P_{unknown}$ reasonably. Then, in model Scenario 2, we use a larger $\gamma_{NO2+h\nu\_ground}$ of $5.3{\cdot}10^{-5}$ and find that the model's performance is significantly improved (Figure S9). The model can accurately predict the HONO peak and well predict the observed HONO diurnal profile. Moreover, laboratory studies suggest that $\gamma_{NO2+h\nu\_ground}$ exhibits an inverse relationship with the NO_2 levels, showing higher values at lower NO_2 concentrations. In Stemmler et al.,[39] the $\gamma_{NO2+h\nu\_ground}$ of $2{\cdot}10^{-5}$ was obtained at 20 ppbv NO_2, much higher than the NO_2 level at the Corsica site (daytime mean: 0.6 ppbv). Hence, a larger $\gamma_{NO2+h\nu\_ground}$ value can be expected for the Corsica site, and the enlarged $P_{NO2+h\nu\_ground}$ is likely to be the main source of $P_{unknown}$. Alternatively, as discussed in Section 3.3, $(S/V)_{ground}$ might be underestimated if SEF is not considered, leading to a similar effect as the underestimation in $\gamma_{NO2+h\nu\_ground}$. For instance, with an SEF of 2.66, the model predicts the same result as that with a $\gamma_{NO2+h\nu\_ground}$ of $5.3{\cdot}10^{-5}$.

We should also note that while a $\gamma_{NO2+h\nu\_ground}$ of $5.3{\cdot}10^{-5}$ or considering an SEF of 2.66 (or any combination where $\gamma_{NO2+h\nu\_ground}$ * SEF = $5.3{\cdot}10^{-5}$) could explain the majority of $P_{unknown}$, there is still a significant gap between predictions and observations during 4:00−10:00 (Figure S9). An even larger

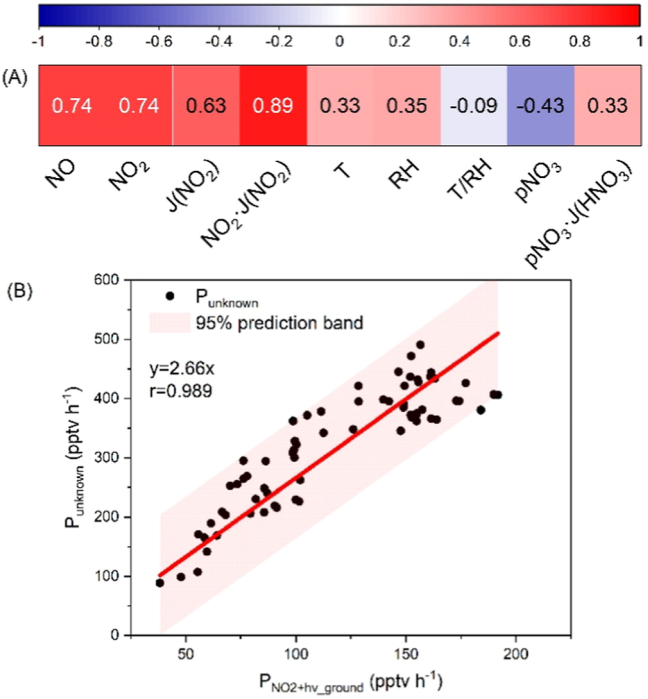

Figure 4. (A) Correlations between $P_{unknown}$ and other parameters and (B) between $P_{unknown}$ and $P_{NO2+h\nu\_ground}$. In panel (A), numbers and the color bar represent the correlation coefficient (r). p-Values for those correlations are <0.01 except for the correlation between $P_{unknown}$ and T/RH.

$\gamma_{NO2+h\nu\_ground}$ or SEF could help reduce the gap, but it is unlikely, as this adjustment would lead to discrepancies during other hours of the day. Moreover, the gap remains with additional consideration of potential primary HONO emissions (S2 + 1% NO_x, Figure S9), which indicates uncertainties in the used parametrizations (e.g., variable MLH in the morning) or the coexistence of other sources.

3.5.2. Biological Soil Emissions. Meusel et al.[9,12] provided an indication of soil HONO emissions in Cyprus, where similar levels of unexplained $P_{unknown}$ were observed. The HONO emission flux (F_{HONO}) from Cyprus soil samples was determined under laboratory conditions. A maximum of 264 ng-N m^{-2} s^{-1} was observed under laboratory conditions and about 7.4 ng-N m^{-2} s^{-1} was estimated for field conditions, which could explain the observed $P_{unknown}$ observed at both Corsica and Cyprus sites. Since both Corsica and Cyprus are Mediterranean islands with similar land cover and vegetation, biological soil HONO emissions could also contribute to the missing HONO source in the present study. Recent laboratory[57−59] and field studies on fertilized soils[60−62] find that F_{HONO} shows a positive correlation with temperature (T) and/or a negative correlation with soil water content or RH. Biological soil emissions become more important when nitrogen fertilizers are applied to agricultural soils,[61,63,64] which is not the case for the soils in the surroundings of the Corsica site. At the Corsica site, $P_{unknown}$ correlates poorly with T, RH, or T/RH (Figures 4 and S11). For instance, during 31 July−3 August, RH was at a low level (average: 45.6 ± 12.6%, Figure S4), but HONO during this period (average: 46.3 ± 33.3 pptv, Figure S2) is even slightly lower than the campaign average (HONO: 56.0 ± 50.8 pptv) with a higher average RH of 69.7 ± 20.0%. On the other hand, our observations are in good agreement with previous flux studies, in which HONO

https://doi.org/10.1021/acs.est.4c11647
Environ. Sci. Technol. XXXX, XXX, XXX−XXX

fluxes were attributed to photosensitized NO_2 uptake on the ground surface[34,65−68] or the photolysis of adsorbed nitrate.[69] In contrast, laboratory experiments revealed the temperature and water content dependencies of biological soil HONO emissions, suggesting a noontime or early afternoon maximum of biological soil HONO emissions. For the uppermost soil layer that controls HONO fluxes, the soil temperature and water content should closely follow solar irradiance and inversely the atmospheric RH (Figure S11), respectively. Due to the difference in the observed and expected diurnal profiles, the biological soil source might coexist but is excluded as the main HONO source at the Corsica site.

3.5.3. Photolysis of Adsorbed HNO_3. During the campaign, HNO_3 was measured by a WAD-IC instrument, and its average was 2.6 ± 1.0 $\mu g\ m^{-3}$ (Figure S6). Using measured concentration and assuming a deposition velocity of 1 cm s^{-1}, integrated deposition to the ground surface during one day of 2200 $\mu g\ m^{-2}$ is calculated. Assuming that all those deposited HNO_3 undergo photolysis with a recommended EF of 7[44] (Table 1) and a HONO yield of 50%,[69−72] the calculated daytime mean HONO production rate would be 68 pptv h^{-1}, representing only a fifth of $P_{unknown}$ (Figure S12). Using a higher EF of 25, the potential maximum HONO production from photolysis of adsorbed HNO_3 would be comparable to observations. However, the significant time misalignment depicted in Figure S12 for the diurnal profiles suggests that photolysis of adsorbed HNO_3 is not the major HONO source in this context.

3.5.4. Other Sources.

a) Photolysis of Particulate Nitrate

As discussed in Section 3.4, with an EF of 7, HONO formation from pNO_3 photolysis ($P_{pNO3+hv}$) makes a minor contribution to daytime HONO formation at the Corsica site. However, reported EF values are prone to large variations. On top of laboratory-reported ones ranging from a single digit to thousands,[70−74] recent field constraints proposed that EF upper limits are not as high as in laboratory studies.[14,44,46,53] Moreover, the poor correlations between $P_{unknown}$ and pNO_3 (r = −0.43, Figure 4) or between $P_{unknown}$ and $pNO_3{\cdot}JHNO_3$ (r = 0.33) also suggest a minor role of pNO_3 in daytime HONO formation. This is also consistent with Friedrich et al., in which pNO_3 photolysis made only minor contributions to ship-based HONO measurements over the Mediterranean Ocean.[7]

b) Acid Displacement

Night-time HONO deposition may constitute a daytime source through acid displacement.[75] This process is limited by the amount of HONO deposited on the soil surface and the abundance of strong acids in the atmosphere.[75] In Corsica, with a night-time HONO level of around 22 pptv, its deposition rate is about 1.6−16 pptv h^{-1} (considering night-time deposition velocities in the range 0.1−1 cm s^{-1}). Assuming that all the deposited HONO at night (20:00−5:00) could be rereleased through acid replacement during the daytime (5:00−20:00), the average HONO production rate through this process would be 1−11 pptv h^{-1}, which would have a negligible impact compared with the observed $P_{unknown}$. In addition, since a maximum of the HNO_3 concentration (the main strong acid for replacement) is observed in the afternoon (Figure S6), followed by consecutive deposition on ground surfaces, the expected diurnal profile of this source will be different from that of $P_{unkonwn}$.

c) Sea-Surface-Derived Source

HONO over the Mediterranean Ocean was measured during the AQABA ship-based campaign in the summer of 2017 and the observed HONO was generally lower than 40 pptv (unpublished data from ref 7), which is much lower than that at the Corsica site (Figure 1), indicating a minor impact of a sea-surface-derived source on HONO levels over island regions. Zhu et al.[14] also observed a similar phenomenon: HONO in marine air was up to one magnitude lower than that in island air, which is reasonable considering the high pH (∼8) and the corresponding high effective solubility of HONO in seawater. Those two studies suggest that in situ HONO formation over the ocean will have only a minor impact on the observed HONO on the island. This is also justified considering that typical transport times from the sea surface to the measurement site were larger than the photolytic lifetime of HONO (Figure S1C).

3.6. Contribution to OH Initiation. Observed during the ChArMex campaign, the reverse diurnal variation of HONO constitutes a significant OH source during the daytime. As shown in Figure 5, compared to OH production from O_3 photolysis, $P(OH)_{O3}$, OH production from HONO, and $P(OH)_{HONO}$ (gross production, estimated as HONO·J(HONO)), starts to rise earlier in the morning, initializing daytime photochemistry. During noontime, $P(OH)_{HONO}$ stabilizes at around 0.5 ppbv h^{-1}, more than one-quarter of $P(OH)_{O3}$. The average relative contribution of $P(OH)_{HONO}$ to

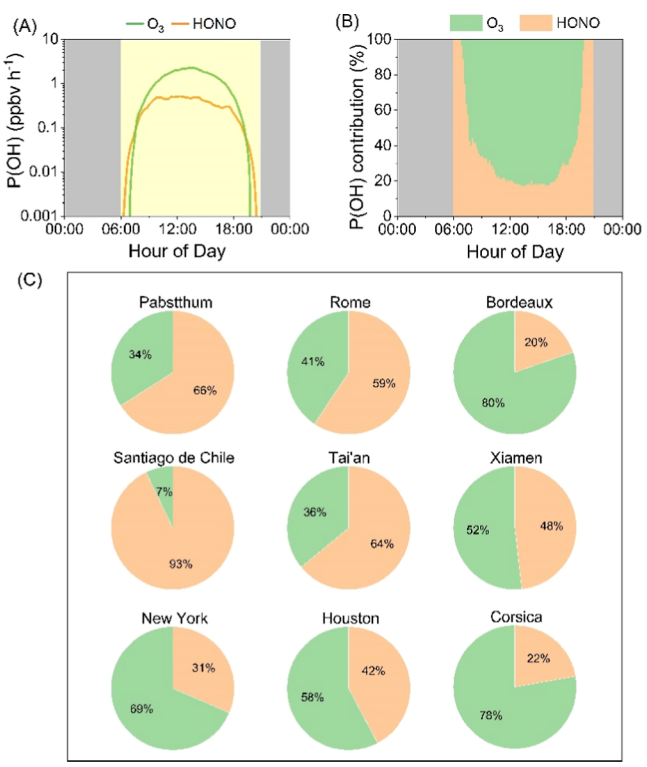

Figure 5. OH production rates from HONO and O_3 photolysis. Average diurnal variations of (A) OH production rates; (B) relative contributions of the two OH sources; and (C) integrated daytime relative contribution of the two OH sources during summer in Pabstthum,[76] Rome,[77] Bordeaux,[78] Santiago de Chile,[79] Tai'an,[28] Xiamen,[80] New York,[81] Houston,[82] and Corsica (this study). Note that only two OH sources (HONO and O_3 photolysis) were considered here for comparison.

https://doi.org/10.1021/acs.est.4c11647
Environ. Sci. Technol. XXXX, XXX, XXX−XXX

$P(OH)_{HONO}$ + $P(OH)_{O3}$ is 39% (17−100%), even comparable to that observed in continental regions in summer (20−90%, Figure 5C), revealing the non-negligible role of HONO in OH production in island regions.

3.7. Atmospheric Implications. *3.7.1. Parameterization Schemes.* Controversies in comprehending HONO formation may arise due to variations in used parametrization schemes. This study offers an overview of various HONO sources, sinks, and related parametrizations, which may serve as a crucial example for future investigations. The results obtained in this study have significant implications for advancing our understanding of HONO chemistry. While a comprehensive ChArMEx data set with a state-of-the-art HONO chemistry parametrization scheme was used, a large part of HONO formation (64%) still could not be explained, leading to a strong unknown source, $P_{unknown}$, up to 470 pptv h^{-1}. From excellent correlations of $P_{unknown}$ with the product of NO_2·JNO_2 or $P_{unknown}$ with $P_{NO2+h\nu\_ground}$, photosensitized NO_2 reactions on the ground surface are likely to account for the $P_{unknown}$ if a larger $\gamma_{NO2+h\nu\_ground}$ is used under low-NO_2 conditions, as expected from $\gamma_{NO2+h\nu\_ground}$ dependencies on NO_2 concentrations. Alternatively, model results can also be improved by considering ground surface roughness, highlighting the need for a more realistic parametrization of ground surfaces.

3.7.2. Reverse Diurnal Profile. The "reverse" diurnal profile of HONO is not unique for island (Figure 2) or marine[8] environments but is also observed in other continental sites, like mountain top,[81,83,84] polar regions,[85−87] remote background regions,[88] and rural forest sites.[69] The common factor for these locations is the low-NO_x environment, which is also characterized by even lower NO_x levels at night compared to daytime. Under these conditions, there is very low night-time HONO buildup resulting from direct combustion sources and/or secondary NO_2 conversion. For the night-time heterogeneous NO_2 conversion, first-order dependence was observed, i.e., the low night-time NO_2 levels also imply slow heterogeneous HONO formation. In contrast, during the daytime, higher uptake coefficients of NO_2 are observed for the photosensitized conversion of NO_2, which are in addition inversely correlated with the NO_2 concentration and may be thus even higher at low-NO_2 conditions compared to lab conditions. Both slow night-time HONO formation and the increasing contribution of photosensitized reaction at low-NO_2 levels contribute to the "atypical" daytime HONO maximum, as observed and discussed in this study. In contrast, when higher NO_2 levels are present in the daytime and when NO_2 in the daytime is lower compared to nighttime (typical for urban conditions), the HONO diurnal profile tends to follow a more "typical" variation, such as the urban coastal sites (e.g., coastal Weybourne, UK,[11] and coastal Qingdao, China[13]) and many urban measurements. At those sites, night-time HONO levels increase due to direct combustion sources and much stronger secondary formation at high-NO_2 levels, which hides smaller photosensitized HONO formation during daytime. Besides the heterogeneous NO_2 conversion proposed in the present study, in very low-NO_x conditions (background sites, open ocean, etc.), additional sources like biological soil emissions[88] and/or particulate nitrate photolysis[8,45] could potentially play a role in the daytime HONO budget.

3.7.3. Marine Atmospheric Oxidizing Capacity. As observed in this work, HONO formation is estimated to contribute significantly to OH production, comparable by strength to the photolysis of ozone. Under a low-NO_x condition such as the marine atmosphere, O_3 production increases with primary OH production and NO concentration.[6] Therefore, HONO photolysis can significantly enhance the production of O_3 by contributing to the formation of both OH and NO. Moreover, longer lifetimes of NO_x and O_3 than HONO allow more extended transport to the surrounding marine atmosphere. Here, islands provide surfaces for heterogeneously converting transported or ship-emitted NO_x to HONO. Both photolysis of HONO and secondarily formed O_3 will potentially enhance the atmospheric oxidizing capacity and further affect the removal of greenhouse gases like methane (CH_4). Hence, our findings suggest that islands may function as an "oxidizing pool", potentially exerting an impact on the surrounding marine atmosphere. The results from the present study underscore the importance of incorporating HONO source parametrization into chemistry-transport and chemistry-climate models and quantifying the corresponding global impact. Furthermore, our results of HONO budget analysis indicate that ground surfaces still significantly affect island HONO measurements both during daytime and at night and thus those measurements may not accurately represent marine conditions. Accordingly, in situ measurements (ship-based or aircraft measurements) over the ocean are needed to better understand the formation of HONO in the marine atmosphere.

■ ASSOCIATED CONTENT

Data Availability Statement

The ChArMEx database is archived at https://mistrals.sedoo.fr/ChArMEx/under the corresponding data and publication policy (https://mistrals.sedoo.fr/ChArMEx/Data-Policy/ChArMEx_DataPolicy.pdf). HONO observations can also be obtained at 10.5281/zenodo.7558756.

Supporting Information

The Supporting Information is available free of charge at https://pubs.acs.org/doi/10.1021/acs.est.4c11647.

Hydrolysis of nitrosyl chloride; box model; instruments providing measurements for this study; worldwide observations used for HONO intercomparison; daytime HONO, HONO/NO_2, and NO_2 plotted against the ratio of the contact time over land (t_{land}) and the lifetime of HONO (τ(HONO)); time series of t_{land}, τ(HONO), and t_{land}/τ(HONO); time series of pNO_3, NO_2, NO, OH, J(HONO), and HONO measured during this campaign; active fire locations on Corsica Island during 11 July−7 August 2013; meteorological measurements (wind direction, WS, atmospheric pressure, solar irradiance, RH, and temperature) during the ChArMEx campaign; wind rose (WS against wind direction) and pollution rose plots (concentration or ratio against wind direction) for HONO, NO_2, pNO_3, NO_x, and HONO/NO_2 during this campaign; average diurnal profiles of HONO, J(HONO), OH, NO_2, NO, particulate nitrate (pNO_3), HNO_3, aerosol surface density ($S_{aerosol}/V$) and O_3; night-time wind rose and pollution rose plots for HONO and HONO/NO_2; sensitivities of γ_{NO2_ground} to $\nu_{deposition}$, MLH, and $\gamma_{NO2\_aerosol}$; diurnal profiles of observed and model HONO; diurnal profiles of $P_{unknown}$ at Corsica and Cyprus sites; average diurnal profiles of $P_{unknown}$, atmospheric temperature (T), RH, and WS;

https://doi.org/10.1021/acs.est.4c11647
Environ. Sci. Technol. XXXX, XXX, XXX−XXX

and $P_{unknown}$ and the calculated HONO production rate from the photolysis of adsorbed HNO_3 (PDF)

AUTHOR INFORMATION

Corresponding Authors

Chaoyang Xue − *Laboratoire de Physique et Chimie de l'Environnement et de l'Espace (LPC2E), CNRS−Université Orléans−CNES, Orléans Cedex 2 45071, France; Max Planck Institute for Chemistry, Mainz 55128, Germany;* orcid.org/0000-0001-6673-7716; Email: ch.xue@mpic.de

Alexandre Kukui − *Laboratoire de Physique et Chimie de l'Environnement et de l'Espace (LPC2E), CNRS−Université Orléans−CNES, Orléans Cedex 2 45071, France;* Email: alexandre.kukui@cnrs-orleans.fr

Authors

Hui Chen − *Institut de Combustion, Aérothermique, Réactivité Environnement (ICARE), CNRS, Orléans Cedex 2 45071, France; School of Environmental and Chemical Engineering, Shanghai University, Shanghai 200444, China;* orcid.org/0000-0002-9785-4744

Max R. McGillen − *Institut de Combustion, Aérothermique, Réactivité Environnement (ICARE), CNRS, Orléans Cedex 2 45071, France*

Hang Su − *Max Planck Institute for Chemistry, Mainz 55128, Germany;* orcid.org/0000-0003-4889-1669

Yafang Cheng − *Max Planck Institute for Chemistry, Mainz 55128, Germany;* orcid.org/0000-0003-4912-9879

Jörg Kleffmann − *Physical and Theoretical Chemistry, University of Wuppertal, Wuppertal 42119, Germany;* orcid.org/0000-0002-7421-0559

Guo Li − *Max Planck Institute for Chemistry, Mainz 55128, Germany*

Mathieu Cazaunau − *Univ Paris Est Creteil and Université Paris Cité, CNRS, LISA, Créteil F-94010, France*

Aurélie Colomb − *Laboratoire de Météorologie Physique (LaMP), Observatoire de Physique du Globe de Clermont-Ferrand, Université Clermont-Auvergne, CNRS, Clermont-Ferrand 63000, France*

Jean Sciare − *Laboratoire des Sciences du Climat et de l'Environnement, Gif-sur-Yvette 91190, France; Climate and Atmosphere Research Center, The Cyprus Institute, Nicosia 2417, Cyprus*

Langley DeWitt − *Aix Marseille University, CNRS, LCE, Marseille 13007, France*

Nicolas Marchand − *Aix Marseille University, CNRS, LCE, Marseille 13007, France*

Roland Sarda-Esteve − *Laboratoire des Sciences du Climat et de l'Environnement, Gif-sur-Yvette 91190, France*

Jean-Eudes Petit − *Laboratoire des Sciences du Climat et de l'Environnement, Gif-sur-Yvette 91190, France;* orcid.org/0000-0003-1516-5927

Complete contact information is available at: https://pubs.acs.org/10.1021/acs.est.4c11647

Author Contributions

C.X. and A.K. led this study and wrote this paper with input from all coauthors. H.C. and M.C. performed HONO and Js measurements. Other authors participated in data collection. All coauthors commented on and approved this manuscript.

Funding

This research has received funding from the French National Research Agency (ANR) project SAFMED (grant ANR-12-BS06−0013). This work is part of the ChArMEx project supported by ADEME, CEA, CNRS-INSU, and Météo-France through the multidisciplinary program MISTRALS (Mediterranean Integrated Studies at Regional And Local Scales). The station at Ersa was partly supported by the CORSiCA project funded by the Collectivité Territoriale de Corse (CTC) through the Fonds Européen de Développement Régional of the European Operational Program 2007−2013 and the Contrat de Plan Etat-Région. This project was also supported by the CaPPA project (Chemical and Physical Properties of the Atmosphere), funded by the French National Research Agency (ANR) through the PIA (Programme d'Investissement d'Avenir) under contract ANR-11-LABX-0005−01 and by the Regional Council Nord-Pas de Calais and the European Funds for Regional Economic Development (FEDER). This work was also supported by LABEX VOLTAIRE ANR-10-LABX-100−01 (2011−20) and the PIVOTS project provided by the Région Centre—Val de Loire (ARD 2020 program and CPER 2015−2020). Open access funded by Max Planck Society.

Notes

The authors declare no competing financial interest.

ACKNOWLEDGMENTS

The authors thank Thierry Bourrianne (Météo-France), Nicolas Bonnaire, José Nicolas, and Anaïs Feron (LSCE) for providing measurement data and support during the campaign. The authors would like to thank Thierry Vincent, Stephane Chevrier, and Gilles Chalumeau from LPC2E for logistical help in preparation and during the campaign, Karine Sartelet from CEREA for managing the SAFMED project, Eric Hamonou and François Dulac from LSCE for managing and coordinating the ChArMEx project, and Nikola Witzel (MPIC) for help on the TOC art. C.X. acknowledges the support from the Alexander von Humboldt Foundation.

REFERENCES

(1) Platt, U.; Perner, D.; Harris, G. W.; Winer, A. M.; Pitts Jr, J. N. Observations of Nitrous Acid in an Urban Atmosphere by Differential Optical Absorption. *Nature* **1980**, *285* (5763), 312−314.

(2) Kleffmann, J. Daytime Sources of Nitrous Acid (HONO) in the Atmospheric Boundary Layer. *ChemPhysChem* **2007**, *8* (8), 1137−1144.

(3) Xue, C. Substantially Growing Interest in the Chemistry of Nitrous Acid (HONO) in China: Current Achievements, Problems, and Future Directions. *Environ. Sci. Technol.* **2022**, *56* (12), 7375−7377.

(4) Spataro, F.; Ianniello, A. Sources of Atmospheric Nitrous Acid: State of the Science, Current Research Needs, and Future Prospects. *J. Air Waste Manage. Assoc.* **2014**, *64* (11), 1232−1250.

(5) Ha, P. T. M.; Kanaya, Y.; Taketani, F.; Andrés Hernández, M. D.; Schreiner, B.; Pfeilsticker, K.; Sudo, K. Implementation of HONO into the Chemistry−Climate Model CHASER (V4.0): Roles in Tropospheric Chemistry. *Geosci. Model Dev.* **2023**, *16* (3), 927−960.

(6) Seinfeld, J. H.; Pandis, S. N. *Atmospheric Chemistry and Physics: From Air Pollution to Climate Change*; John Wiley & Sons, 2016.

(7) Friedrich, N.; Eger, P.; Shenolikar, J.; Sobanski, N.; Schuladen, J.; Dienhart, D.; Hottmann, B.; Tadic, I.; Fischer, H.; Martinez, M.; Rohloff, R.; Tauer, S.; Harder, H.; Pfannerstill, E. Y.; Wang, N.; Williams, J.; Brooks, J.; Drewnick, F.; Su, H.; Li, G.; Cheng, Y.; Lelieveld, J.; Crowley, J. N. Reactive Nitrogen around the Arabian Peninsula and in the Mediterranean Sea during the 2017 AQABA Ship Campaign. *Atmos. Chem. Phys.* **2021**, *21* (10), 7473−7498.

https://doi.org/10.1021/acs.est.4c11647
Environ. Sci. Technol. XXXX, XXX, XXX−XXX

(8) Ye, C.; Zhou, X.; Pu, D.; Stutz, J.; Festa, J.; Spolaor, M.; Tsai, C.; Cantrell, C.; Mauldin, R. L.; Campos, T.; Weinheimer, A.; Hornbrook, R. S.; Apel, E. C.; Guenther, A.; Kaser, L.; Yuan, B.; Karl, T.; Haggerty, J.; Hall, S.; Ullmann, K.; Smith, J. N.; Ortega, J.; Knote, C. Rapid Cycling of Reactive Nitrogen in the Marine Boundary Layer. *Nature* **2016**, *532* (7600), 489−491.
(9) Meusel, H.; Kuhn, U.; Reiffs, A.; Mallik, C.; Harder, H.; Martinez, M.; Schuladen, J.; Bohn, B.; Parchatka, U.; Crowley, J. N.; Fischer, H.; Tomsche, L.; Novelli, A.; Hoffmann, T.; Janssen, R. H. H.; Hartogensis, O.; Pikridas, M.; Vrekoussis, M.; Bourtsoukidis, E.; Weber, B.; Lelieveld, J.; Williams, J.; Pöschl, U.; Cheng, Y.; Su, H. Daytime Formation of Nitrous Acid at a Coastal Remote Site in Cyprus Indicating a Common Ground Source of Atmospheric HONO and NO. *Atmos. Chem. Phys.* **2016**, *16* (22), 14475−14493.
(10) Yang, J.; Shen, H.; Guo, M.-Z.; Zhao, M.; Jiang, Y.; Chen, T.; Liu, Y.; Li, H.; Zhu, Y.; Meng, H.; Wang, W.; Xue, L. Strong Marine-Derived Nitrous Acid (HONO) Production Observed in the Coastal Atmosphere of Northern China. *Atmos. Environ.* **2021**, *244*, 117948.
(11) Crilley, L. R.; Kramer, L. J.; Pope, F. D.; Reed, C.; Lee, J. D.; Carpenter, L. J.; Hollis, L. D. J.; Ball, S. M.; Bloss, W. J. Is the Ocean Surface a Source of Nitrous Acid (HONO) in the Marine Boundary Layer? *Atmos. Chem. Phys.* **2021**, *21* (24), 18213−18225.
(12) Meusel, H.; Tamm, A.; Kuhn, U.; Wu, D.; Leifke, A. L.; Fiedler, S.; Ruckteschler, N.; Yordanova, P.; Lang-Yona, N.; Pöhlker, M.; Lelieveld, J.; Hoffmann, T.; Pöschl, U.; Su, H.; Weber, B.; Cheng, Y. Emission of Nitrous Acid from Soil and Biological Soil Crusts Represents an Important Source of HONO in the Remote Atmosphere in Cyprus. *Atmos. Chem. Phys.* **2018**, *18* (2), 799−813.
(13) Wen, L.; Chen, T.; Zheng, P.; Wu, L.; Wang, X.; Mellouki, A.; Xue, L.; Wang, W. Nitrous Acid in Marine Boundary Layer over Eastern Bohai Sea, China: Characteristics, Sources, and Implications. *Sci. Total Environ.* **2019**, *670*, 282−291.
(14) Zhu, Y.; Wang, Y.; Zhou, X.; Elshorbany, Y. F.; Ye, C.; Hayden, M.; Peters, A. J. An Investigation into the Chemistry of HONO in the Marine Boundary Layer at Tudor Hill Marine Atmospheric Observatory in Bermuda. *Atmos. Chem. Phys.* **2022**, *22* (9), 6327−6346.
(15) Michoud, V.; Sciare, J.; Sauvage, S.; Dusanter, S.; Léonardis, T.; Gros, V.; Kalogridis, C.; Zannoni, N.; Féron, A.; Petit, J.-E.; Crenn, V.; Baisnée, D.; Sarda-Estève, R.; Bonnaire, N.; Marchand, N.; DeWitt, H. L.; Pey, J.; Colomb, A.; Gheusi, F.; Szidat, S.; Stavroulas, I.; Borbon, A.; Locoge, N. Organic Carbon at a Remote Site of the Western Mediterranean Basin: Sources and Chemistry during the ChArMEx SOP2 Field Experiment. *Atmos. Chem. Phys.* **2017**, *17* (14), 8837−8865.
(16) Kukui, A.; Chartier, M.; Wang, J.; Chen, H.; Dusanter, S.; Sauvage, S.; Michoud, V.; Locoge, N.; Gros, V.; Bourrianne, T.; Sellegri, K.; Pichon, J.-M. Role of Criegee Intermediates in the Formation of Sulfuric Acid at a Mediterranean (Cape Corsica) Site under Influence of Biogenic Emissions. *Atmos. Chem. Phys.* **2021**, *21* (17), 13333−13351.
(17) Heland, J.; Kleffmann, J.; Kurtenbach, R.; Wiesen, P. A New Instrument To Measure Gaseous Nitrous Acid (HONO) in the Atmosphere. *Environ. Sci. Technol.* **2001**, *35* (15), 3207−3212.
(18) Kleffmann, J.; Lörzer, J. C.; Wiesen, P.; Kern, C.; Trick, S.; Volkamer, R.; Rodenas, M.; Wirtz, K. Intercomparison of the DOAS and LOPAP Techniques for the Detection of Nitrous Acid (HONO). *Atmos. Environ.* **2006**, *40* (20), 3640−3652.
(19) Kukui, A.; Legrand, M.; Preunkert, S.; Frey, M. M.; Loisil, R.; Gil Roca, J.; Jourdain, B.; King, M. D.; France, J. L.; Ancellet, G. Measurements of OH and RO_2 Radicals at Dome C, East Antarctica. *Atmos. Chem. Phys.* **2014**, *14* (22), 12373−12392.
(20) Petetin, H.; Sciare, J.; Bressi, M.; Gros, V.; Rosso, A.; Sanchez, O.; Sarda-Estève, R.; Petit, J.-E.; Beekmann, M. Assessing the Ammonium Nitrate Formation Regime in the Paris Megacity and Its Representation in the CHIMERE Model. *Atmos. Chem. Phys.* **2016**, *16* (16), 10419−10440.
(21) Crilley, L. R.; Kramer, L.; Pope, F. D.; Whalley, L. K.; Cryer, D. R.; Heard, D. E.; Lee, J. D.; Reed, C.; Bloss, W. J. On the Interpretation of in Situ HONO Observations via Photochemical Steady State. *Faraday Discuss.* **2016**, *189*, 191−212.
(22) Kleffmann, J.; Gavriloaiei, T.; Hofzumahaus, A.; Holland, F.; Koppmann, R.; Rupp, L.; Schlosser, E.; Siese, M.; Wahner, A. Daytime Formation of Nitrous Acid: A Major Source of OH Radicals in a Forest. *Geophys. Res. Lett.* **2005**, *32* (5), L05818.
(23) Theys, N.; Volkamer, R.; Müller, J.-F.; Zarzana, K. J.; Kille, N.; Clarisse, L.; De Smedt, I.; Lerot, C.; Finkenzeller, H.; Hendrick, F.; Koenig, T. K.; Lee, C. F.; Knote, C.; Yu, H.; Van Roozendael, M. Global Nitrous Acid Emissions and Levels of Regional Oxidants Enhanced by Wildfires. *Nat. Geosci.* **2020**, *13* (10), 681−686.
(24) Peng, Q.; Palm, B. B.; Melander, K. E.; Lee, B. H.; Hall, S. R.; Ullmann, K.; Campos, T.; Weinheimer, A. J.; Apel, E. C.; Hornbrook, R. S.; Hills, A. J.; Montzka, D. D.; Flocke, F.; Hu, L.; Permar, W.; Wielgasz, C.; Lindaas, J.; Pollack, I. B.; Fischer, E. V.; Bertram, T. H.; Thornton, J. A. HONO Emissions from Western U.S. Wildfires Provide Dominant Radical Source in Fresh Wildfire Smoke. *Environ. Sci. Technol.* **2020**, *54* (10), 5954−5963.
(25) Burling, I. R.; Yokelson, R. J.; Akagi, S. K.; Urbanski, S. P.; Wold, C. E.; Griffith, D. W. T.; Johnson, T. J.; Reardon, J.; Weise, D. R. Airborne and Ground-Based Measurements of the Trace Gases and Particles Emitted by Prescribed Fires in the United States. *Atmos. Chem. Phys.* **2011**, *11* (23), 12197−12216.
(26) Bejan, I.; Abd El Aal, Y.; Barnes, I.; Benter, T.; Bohn, B.; Wiesen, P.; Kleffmann, J. The Photolysis of Ortho-Nitrophenols: A New Gas Phase Source of HONO. *Phys. Chem. Chem. Phys.* **2006**, *8* (17), 2028−2035.
(27) Xue, C.; Zhang, C.; Ye, C.; Liu, P.; Catoire, V.; Krysztofiak, G.; Chen, H.; Ren, Y.; Zhao, X.; Wang, J.; Zhang, F.; Zhang, C.; Zhang, J.; An, J.; Wang, T.; Chen, J.; Kleffmann, J.; Mellouki, A.; Mu, Y. HONO Budget and Its Role in Nitrate Formation in the Rural North China Plain. *Environ. Sci. Technol.* **2020**, *54* (18), 11048−11057.
(28) Xue, C.; Ye, C.; Kleffmann, J.; Zhang, W.; He, X.; Liu, P.; Zhang, C.; Zhao, X.; Liu, C.; Ma, Z.; Liu, J.; Wang, J.; Lu, K.; Catoire, V.; Mellouki, A.; Mu, Y. Atmospheric Measurements at Mt. Tai − Part II: HONO Budget and Radical (RO_x + NO_3) Chemistry in the Lower Boundary Layer. *Atmos. Chem. Phys.* **2022**, *22* (2), 1035−1057.
(29) Wong, K. W.; Tsai, C.; Lefer, B.; Grossberg, N.; Stutz, J. Modeling of Daytime HONO Vertical Gradients during SHARP 2009. *Atmos. Chem. Phys.* **2013**, *13* (7), 3587−3601.
(30) Wong, K. W.; Oh, H. J.; Lefer, B. L.; Rappenglück, B.; Stutz, J. Vertical Profiles of Nitrous Acid in the Nocturnal Urban Atmosphere of Houston, TX. *Atmos. Chem. Phys.* **2011**, *11*, 3595−3609.
(31) Stutz, J.; Alicke, B.; Neftel, A. Nitrous Acid Formation in the Urban Atmosphere: Gradient Measurements of NO_2 and HONO over Grass in Milan, Italy. *J. Geophys. Res. Atmos.* **2002**, *107* (D22), 8192.
(32) Schimang, R.; Folkers, A.; Kleffmann, J.; Kleist, E.; Miebach, M.; Wildt, J. Uptake of Gaseous Nitrous Acid (HONO) by Several Plant Species. *Atmos. Environ.* **2006**, *40* (7), 1324−1335.
(33) Vandenboer, T. C.; Brown, S. S.; Murphy, J. G.; Keene, W. C.; Young, C. J.; Pszenny, A. A. P.; Kim, S.; Warneke, C.; de Gouw, J. A.; Maben, J. R.; Wagner, N. L.; Riedel, T. P.; Thornton, J. A.; Wolfe, D. E.; Dubé, W. P.; Öztürk, F.; Brock, C. A.; Grossberg, N.; Lefer, B.; Lerner, B.; Middlebrook, A. M.; Roberts, J. M. Understanding the Role of the Ground Surface in HONO Vertical Structure: High Resolution Vertical Profiles during NACHTT-11. *J. Geophys. Res. Atmos.* **2013**, *118* (17), 10155−10171.
(34) Laufs, S.; Cazaunau, M.; Stella, P.; Kurtenbach, R.; Cellier, P.; Mellouki, A.; Loubet, B.; Kleffmann, J. Diurnal Fluxes of HONO above a Crop Rotation. *Atmos. Chem. Phys.* **2017**, *17* (11), 6907−6923.
(35) Vogel, B.; Vogel, H.; Kleffmann, J.; Kurtenbach, R. Measured and Simulated Vertical Profiles of Nitrous Acid - Part II. Model Simulations and Indications for a Photolytic Source. *Atmos. Environ.* **2003**, *37* (21), 2957−2966.
(36) Stemmler, K.; Ndour, M.; Elshorbany, Y.; Kleffmann, J.; D'Anna, B.; George, C.; Bohn, B.; Ammann, M. Light Induced

https://doi.org/10.1021/acs.est.4c11647
Environ. Sci. Technol. XXXX, XXX, XXX−XXX

Conversion of Nitrogen Dioxide into Nitrous Acid on Submicron Humic Acid Aerosol. *Atmos. Chem. Phys.* **2007**, *7* (16), 4237−4248.
(37) Kleffmann, J.; Becker, K. H.; Wiesen, P. Heterogeneous NO_2 Conversion Processes on Acid Surfaces: Possible Atmospheric Implications. *Atmos. Environ.* **1998**, *32* (16), 2721−2729.
(38) Kurtenbach, R.; Becker, K. H.; Gomes, J. A. G.; Kleffmann, J.; Lörzer, J. C.; Spittler, M.; Wiesen, P.; Ackermann, R.; Geyer, A.; Platt, U. Investigations of Emissions and Heterogeneous Formation of HONO in a Road Traffic Tunnel. *Atmos. Environ.* **2001**, *35* (20), 3385−3394.
(39) Stemmler, K.; Ammann, M.; Donders, C.; Kleffmann, J.; George, C. Photosensitized Reduction of Nitrogen Dioxide on Humic Acid as a Source of Nitrous Acid. *Nature* **2006**, *440* (7081), 195−198.
(40) Yang, W.; Han, C.; Zhang, T.; Tang, N.; Yang, H.; Xue, X. Heterogeneous Photochemical Uptake of NO_2 on the Soil Surface as an Important Ground-Level HONO Source. *Environ. Pollut.* **2021**, *271* (2), 116289.
(41) Han, C.; Yang, W.; Wu, Q.; Yang, H.; Xue, X. Heterogeneous Photochemical Conversion of NO_2 to HONO on the Humic Acid Surface under Simulated Sunlight. *Environ. Sci. Technol.* **2016**, *50* (10), 5017−5023.
(42) Harrison, R. M.; Collins, G. M. Measurements of Reaction Coefficients of NO_2 and HONO on Aerosol Particles. *J. Atmos. Chem.* **1998**, *30* (3), 397−406.
(43) Li, M.; Su, H.; Li, G.; Ma, N.; Pöschl, U.; Cheng, Y. Relative Importance of Gas Uptake on Aerosol and Ground Surfaces Characterized by Equivalent Uptake Coefficients. *Atmos. Chem. Phys.* **2019**, *19* (16), 10981−11011.
(44) Romer, P. S.; Wooldridge, P. J.; Crounse, J. D.; Kim, M. J.; Wennberg, P. O.; Dibb, J. E.; Scheuer, E.; Blake, D. R.; Meinardi, S.; Brosius, A. L.; Thames, A. B.; Miller, D. O.; Brune, W. H.; Hall, S. R.; Ryerson, T. B.; Cohen, R. C. Constraints on Aerosol Nitrate Photolysis as a Potential Source of HONO and NO_X. *Environ. Sci. Technol.* **2018**, *52* (23), 13738−13746.
(45) Andersen, S. T.; Carpenter, L. J.; Reed, C.; Lee, J. D.; Chance, R.; Sherwen, T.; Vaughan, A. R.; Stewart, J.; Edwards, P. M.; Bloss, W. J.; Sommariva, R.; Crilley, L. R.; Nott, G. J.; Neves, L.; Read, K.; Heard, D. E.; Seakins, P. W.; Whalley, L. K.; Boustead, G. A.; Fleming, L. T.; Stone, D.; Fomba, K. W. Extensive Field Evidence for the Release of HONO from the Photolysis of Nitrate Aerosols. *Sci. Adv.* **2023**, *9* (3), 1−9.
(46) Peng, Q.; Palm, B. B.; Fredrickson, C. D.; Lee, B. H.; Hall, S. R.; Ullmann, K.; Weinheimer, A. J.; Levin, E.; DeMott, P.; Garofalo, L. A.; Pothier, M. A.; Farmer, D. K.; Fischer, E. V.; Thornton, J. A. Direct Constraints on Secondary HONO Production in Aged Wildfire Smoke From Airborne Measurements Over the Western US. *Geophys. Res. Lett.* **2022**, *49* (15), 1−10.
(47) Michoud, V.; Colomb, A.; Borbon, A.; Miet, K.; Beekmann, M.; Camredon, M.; Aumont, B.; Perrier, S.; Zapf, P.; Siour, G.; Ait-Helal, W.; Afif, C.; Kukui, A.; Furger, M.; Dupont, J. C.; Haeffelin, M.; Doussin, J. F. Study of the Unknown HONO Daytime Source at a European Suburban Site during the MEGAPOLI Summer and Winter Field Campaigns. *Atmos. Chem. Phys.* **2014**, *14* (6), 2805−2822.
(48) Lee, J. D.; Whalley, L. K.; Heard, D. E.; Stone, D.; Dunmore, R. E.; Hamilton, J. F.; Young, D. E.; Allan, J. D.; Laufs, S.; Kleffmann, J. Detailed Budget Analysis of HONO in Central London Reveals a Missing Daytime Source. *Atmos. Chem. Phys.* **2016**, *16* (5), 2747−2764.
(49) Singh, A.; Crilley, L. R.; Pope, F. D.; Bloss, W. J. Insights into HONO Sources from Observations during a Solar Eclipse. *Environ. Sci. Atmos* **2021**, *1* (6), 395−405.
(50) Song, Y.; Zhang, Y.; Xue, C.; Liu, P.; He, X.; Li, X.; Mu, Y. The Seasonal Variations and Potential Sources of Nitrous Acid (HONO) in the Rural North China Plain. *Environ. Pollut.* **2022**, *311*, 119967.
(51) Ye, C.; Zhou, X.; Pu, D.; Stutz, J.; Festa, J.; Spolaor, M.; Tsai, C.; Cantrell, C.; Mauldin III, R. L.; Weinheimer, A.; Hornbrook, R. S.; Apel, E. C.; Guenther, A.; Kaser, L.; Yuan, B.; Karl, T.; Haggerty, J.; Hall, S.; Ullmann, K.; Smith, J.; Ortega, J. Tropospheric HONO Distribution and Chemistry in the Southeastern US. *Atmos. Chem. Phys.* **2018**, *18* (12), 9107−9120.
(52) Neuman, J. A.; Trainer, M.; Brown, S. S.; Min, K.-E.; Nowak, J. B.; Parrish, D. D.; Peischl, J.; Pollack, I. B.; Roberts, J. M.; Ryerson, T. B.; Veres, P. R. HONO Emission and Production Determined from Airborne Measurements over the Southeast U.S. *J. Geophys. Res. Atmos.* **2016**, *121* (15), 9237−9250.
(53) Xue, C.; Ye, C.; Kleffmann, J.; Zhang, C.; Catoire, V.; Bao, F.; Mellouki, A.; Xue, L.; Chen, J.; Lu, K.; Zhao, Y.; Liu, H.; Guo, Z.; Mu, Y. Atmospheric Measurements at Mt. Tai − Part I: HONO Formation and Its Role in the Oxidizing Capacity of the Upper Boundary Layer. *Atmos. Chem. Phys.* **2022**, *22* (5), 3149−3167.
(54) Kebede, M. A.; Bish, D. L.; Losovyj, Y.; Engelhard, M. H.; Raff, J. D. The Role of Iron-Bearing Minerals in NO_2 to HONO Conversion on Soil Surfaces. *Environ. Sci. Technol.* **2016**, *50* (16), 8649−8660.
(55) Stutz, J.; Alicke, B.; Ackermann, R.; Geyer, A.; Wang, S.; White, A. B.; Williams, E. J.; Spicer, C. W.; Fast, J. D. Relative Humidity Dependence of HONO Chemistry in Urban Areas. *J. Geophys. Res. Atmos.* **2004**, *109* (D3), D03307.
(56) Ammann, M.; Rössler, E.; StrekowskiPresent address Universi, R.; George, C. Nitrogen Dioxide Multiphase Chemistry: Uptake Kinetics on Aqueous Solutions Containing Phenolic Compounds. *Phys. Chem. Chem. Phys.* **2005**, *7* (12), 2513−2518.
(57) Su, H.; Cheng, Y.; Oswald, R.; Behrendt, T.; Trebs, I.; Meixner, F. X.; Andreae, M. O.; Cheng, P.; Zhang, Y.; Pöschl, U. Soil Nitrite as a Source of Atmospheric HONO and OH Radicals. *Science* **2011**, *333* (6049), 1616−1618.
(58) Oswald, R.; Behrendt, T.; Ermel, M.; Wu, D.; Su, H.; Cheng, Y.; Breuninger, C.; Moravek, A.; Mougin, E.; Delon, C.; Loubet, B.; Pommerening-Röser, A.; Sörgel, M.; Pöschl, U.; Hoffmann, T.; Andreae, M. O.; Meixner, F. X.; Trebs, I. HONO Emissions from Soil Bacteria as a Major Source of Atmospheric Reactive Nitrogen. *Science* **2013**, *341* (6151), 1233−1235.
(59) Bao, F.; Cheng, Y.; Kuhn, U.; Li, G.; Wang, W.; Kratz, A. M.; Weber, J.; Weber, B.; Pöschl, U.; Su, H. Key Role of Equilibrium HONO Concentration over Soil in Quantifying Soil−Atmosphere HONO Fluxes. *Environ. Sci. Technol.* **2022**, *56* (4), 2204−2212.
(60) Xue, C.; Ye, C.; Zhang, Y.; Ma, Z.; Liu, P.; Zhang, C.; Zhao, X.; Liu, J.; Mu, Y. Development and Application of a Twin Open-Top Chambers Method to Measure Soil HONO Emission in the North China Plain. *Sci. Total Environ.* **2019**, *659*, 621−631.
(61) Xue, C.; Ye, C.; Zhang, C.; Catoire, V.; Liu, P.; Gu, R.; Zhang, J.; Ma, Z.; Zhao, X.; Zhang, W.; Ren, Y.; Krysztofiak, G.; Tong, S.; Xue, L.; An, J.; Ge, M.; Mellouki, A.; Mu, Y. Evidence for Strong HONO Emission from Fertilized Agricultural Fields and Its Remarkable Impact on Regional O_3 Pollution in the Summer North China Plain. *ACS Earth Sp. Chem.* **2021**, *5* (2), 340−347.
(62) Tang, K.; Qin, M.; Duan, J.; Fang, W.; Meng, F.; Liang, S.; Xie, P.; Liu, J.; Liu, W.; Xue, C.; Mu, Y. A Dual Dynamic Chamber System Based on IBBCEAS for Measuring Fluxes of Nitrous Acid in Agricultural Fields in the North China Plain. *Atmos. Environ.* **2019**, *196*, 10−19.
(63) Song, Y.; Xue, C.; Zhang, Y.; Liu, P.; Bao, F.; Li, X.; Mu, Y. Measurement Report: Exchange Fluxes of HONO over Agricultural Fields in the North China Plain. *Atmos. Chem. Phys.* **2023**, *23* (24), 15733−15747.
(64) Ramsay, R.; Di Marco, C. F.; Heal, M. R.; Twigg, M. M.; Cowan, N.; Jones, M. R.; Leeson, S. R.; Bloss, W. J.; Kramer, L. J.; Crilley, L.; Sörgel, M.; Andreae, M.; Nemitz, E. Surface-Atmosphere Exchange of Inorganic Water-Soluble Gases and Associated Ions in Bulk Aerosol above Agricultural Grassland Pre- and Postfertilisation. *Atmos. Chem. Phys.* **2018**, *18* (23), 16953−16978.
(65) Harrison, R. M.; Kitto, A.-M. N. Evidence for a Surface Source of Atmospheric Nitrous Acid. *Atmos. Environ.* **1994**, *28* (6), 1089−1094.
(66) Ren, X.; Sanders, J. E.; Rajendran, A.; Weber, R. J.; Goldstein, A. H.; Pusede, S. E.; Browne, E. C.; Min, K. E.; Cohen, R. C. A

https://doi.org/10.1021/acs.est.4c11647
Environ. Sci. Technol. XXXX, XXX, XXX−XXX

Relaxed Eddy Accumulation System for Measuring Vertical Fluxes of Nitrous Acid. *Atmos. Meas. Tech.* **2011**, *4* (10), 2093−2103.
(67) Meng, F.; Qin, M.; Fang, W.; Duan, J.; Tang, K.; Zhang, H.; Shao, D.; Liao, Z.; Feng, Y.; Huang, Y.; Ni, T.; Xie, P.; Liu, J.; Liu, W. Measurement of HONO Flux Using the Aerodynamic Gradient Method over an Agricultural Field in the Huaihe River Basin, China. *J. Environ. Sci.* **2022**, *114*, 297−307.
(68) von der Heyden, L.; Wißdorf, W.; Kurtenbach, R.; Kleffmann, J. A Relaxed Eddy Accumulation (REA) LOPAP System for Flux Measurements of Nitrous Acid (HONO). *Atmos. Meas. Tech.* **2022**, *15* (6), 1983−2000.
(69) Zhou, X.; Zhang, N.; TerAvest, M.; Tang, D.; Hou, J.; Bertman, S.; Alaghmand, M.; Shepson, P. B.; Carroll, M. A.; Griffith, S.; Dusanter, S.; Stevens, P. S. Nitric Acid Photolysis on Forest Canopy Surface as a Source for Tropospheric Nitrous Acid. *Nat. Geosci.* **2011**, *4* (7), 440−443.
(70) Laufs, S.; Kleffmann, J. Investigations on HONO Formation from Photolysis of Adsorbed HNO_3 on Quartz Glass Surfaces. *Phys. Chem. Chem. Phys.* **2016**, *18* (14), 9616−9625.
(71) Ye, C.; Zhang, N.; Gao, H.; Zhou, X. Photolysis of Particulate Nitrate as a Source of HONO and NO_X. *Environ. Sci. Technol.* **2017**, *51* (12), 6849−6856.
(72) Bao, F.; Li, M.; Zhang, Y.; Chen, C.; Zhao, J. Photochemical Aging of Beijing Urban $PM_{2.5}$: HONO Production. *Environ. Sci. Technol.* **2018**, *52* (11), 6309−6316.
(73) Wang, X.; Dalton, E. Z.; Payne, Z. C.; Perrier, S.; Riva, M.; Raff, J. D.; George, C. Superoxide and Nitrous Acid Production from Nitrate Photolysis Is Enhanced by Dissolved Aliphatic Organic Matter. *Environ. Sci. Technol. Lett.* **2021**, *8* (1), 53−58.
(74) Shi, Q.; Tao, Y.; Krechmer, J. E.; Heald, C. L.; Murphy, J. G.; Kroll, J. H.; Ye, Q. Laboratory Investigation of Renoxification from the Photolysis of Inorganic Particulate Nitrate. *Environ. Sci. Technol.* **2021**, *55* (2), 854−861.
(75) Vandenboer, T. C.; Young, C. J.; Talukdar, R. K.; Markovic, M. Z.; Brown, S. S.; Roberts, J. M.; Murphy, J. G. Nocturnal Loss and Daytime Source of Nitrous Acid through Reactive Uptake and Displacement. *Nat. Geosci.* **2015**, *8* (1), 55−60.
(76) Alicke, B.; Geyer, A.; Hofzumahaus, A.; Holland, F.; Konrad, S.; Pätz, H.-W.; Schäfer, J.; Stutz, J.; Volz-Thomas, A.; Platt, U. OH Formation by HONO Photolysis during the BERLIOZ Experiment. *J. Geophys. Res. Atmos.* **2003**, *108* (D4), 8247.
(77) Acker, K.; Febo, A.; Trick, S.; Perrino, C.; Bruno, P.; Wiesen, P.; Möller, D.; Wieprecht, W.; Auel, R.; Giusto, M.; Geyer, A.; Platt, U.; Allegrini, I. Nitrous Acid in the Urban Area of Rome. *Atmos. Environ.* **2006**, *40* (17), 3123−3133.
(78) Wang, X.; Li, D.; Flaud, P.; Li, H.; Perrier, S.; Villenave, E.; Dusanter, S.; Tomas, A.; Perraudin, E.; George, C.; Riva, M. Atmospheric Nitrous Acid Measurement in the French Landes Forest. *ACS Earth Sp. Chem.* **2022**, *6* (1), 25−33.
(79) Elshorbany, Y. F.; Kleffmann, J.; Kurtenbach, R.; Lissi, E.; Rubio, M.; Villena, G.; Gramsch, E.; Rickard, A. R.; Pilling, M. J.; Wiesen, P. Seasonal Dependence of the Oxidation Capacity of the City of Santiago de Chile. *Atmos. Environ.* **2010**, *44* (40), 5383−5394.
(80) Hu, B.; Duan, J.; Hong, Y.; Xu, L.; Li, M.; Bian, Y.; Qin, M.; Fang, W.; Xie, P.; Chen, J. Exploration of the Atmospheric Chemistry of Nitrous Acid in a Coastal City of Southeastern China: Results from Measurements across Four Seasons. *Atmos. Chem. Phys.* **2022**, *22* (1), 371−393.
(81) Zhou, X.; Huang, G.; Civerolo, K.; Roychowdhury, U.; Demerjian, K. L. Summertime Observations of HONO, HCHO, and O_3 at the Summit of Whiteface Mountain, New York. *J. Geophys. Res. Atmos.* **2007**, *112* (8), 1−13.
(82) Ren, X.; Van Duin, D.; Cazorla, M.; Chen, S.; Mao, J.; Zhang, L.; Brune, W. H.; Flynn, J. H.; Grossberg, N.; Lefer, B. L.; Rappenglück, B.; Wong, K. W.; Tsai, C.; Stutz, J.; Dibb, J. E.; Thomas Jobson, B.; Luke, W. T.; Kelley, P. Atmospheric Oxidation Chemistry and Ozone Production: Results from SHARP 2009 in Houston, Texas. *J. Geophys. Res. Atmos.* **2013**, *118* (11), 5770−5780.
(83) Acker, K.; Möller, D.; Wieprecht, W.; Meixner, F. X.; Bohn, B.; Gilge, S.; Plass-Dülmer, C.; Berresheim, H. Strong Daytime Production of OH from HNO_2 at a Rural Mountain Site. *Geophys. Res. Lett.* **2006**, *33* (2), L02809.
(84) Kleffmann, J.; Wiesen, P. Technical Note: Quantification of Interferences of Wet Chemical HONO LOPAP Measurements under Simulated Polar Conditions. *Atmos. Chem. Phys.* **2008**, *8* (22), 6813−6822.
(85) Bond, A. M. H.; Frey, M. M.; Kaiser, J.; Kleffmann, J.; Jones, A. E.; Squires, F. A. Snowpack Nitrate Photolysis Drives the Summertime Atmospheric Nitrous Acid (HONO) Budget in Coastal Antarctica. *Atmos. Chem. Phys.* **2023**, *23* (9), 5533−5550.
(86) Villena, G.; Wiesen, P.; Cantrell, C. A.; Flocke, F.; Fried, A.; Hall, S. R.; Hornbrook, R. S.; Knapp, D.; Kosciuch, E.; Mauldin, R. L.; McGrath, J. A.; Montzka, D.; Richter, D.; Ullmann, K.; Walega, J.; Weibring, P.; Weinheimer, A.; Staebler, R. M.; Liao, J.; Huey, L. G.; Kleffmann, J. Nitrous Acid (HONO) during Polar Spring in Barrow, Alaska: A Net Source of OH Radicals? *J. Geophys. Res. Atmos.* **2011**, *116* (24), D00R07.
(87) Zhou, X.; Beine, H. J.; Honrath, R. E.; Fuentes, J. D.; Simpson, W.; Shepson, P. B.; Bottenheim, J. W. Snowpack Photochemical Production of HONO: A Major Source of OH in the Arctic Boundary Layer in Springtime. *Geophys. Res. Lett.* **2001**, *28* (21), 4087−4090.
(88) Wang, J.; Zhang, Y.; Zhang, C.; Wang, Y.; Zhou, J.; Whalley, L. K.; Slater, E. J.; Dyson, J. E.; Xu, W.; Cheng, P.; Han, B.; Wang, L.; Yu, X.; Wang, Y.; Woodward-Massey, R.; Lin, W.; Zhao, W.; Zeng, L.; Ma, Z.; Heard, D. E.; Ye, C. Validating HONO as an Intermediate Tracer of the External Cycling of Reactive Nitrogen in the Background Atmosphere. *Environ. Sci. Technol.* **2023**, *57* (13), 5474−5484.

https://doi.org/10.1021/acs.est.4c11647
Environ. Sci. Technol. XXXX, XXX, XXX−XXX